Multiple Scattering in Discrete Random Media Using First-Order Incoherent Interactions

Muinonen, Karri; Markkanen, Johannes; Väisänen, Timo; Peltoniemi, Jouni I.; Penttilä, Antti

2017-11
Wiley Blackwell
http://hdl.handle.net/10138/229841
Muinonen, K, Markkanen, J, Väisänen, T, Peltoniemi, J I & Penttilä, A 2017, 'Multiple Scattering in Discrete Random Media Using First-Order Incoherent Interactions', Radio Science, vol. 52, no. 11, pp. 1419-1431. https://doi.org/10.1002/2017RS006419

AGU PUBLICATIONS

Radio Science

RESEARCH ARTICLE
10.1002/2017RS006419

Special Section:
Special Issue of the 2016 URSI Commission B International Symposium on Electromagnetic Theory

Multiple Scattering in Discrete Random Media Using First-Order Incoherent Interactions

K. Muinonen[1,2], J. Markkanen[1], T. Väisänen[1], J. I. Peltoniemi[2], and A. Penttilä[1]

[1]Department of Physics, University of Helsinki, Helsinki, Finland, [2]Finnish Geospatial Research Institute, National Land Survey of Finland, Helsinki, Finland

Key Points:
- We introduce incoherent extinction, scattering, and absorption into the radiative transfer coherent backscattering method (RT-CB)
- Consequently, we extend the applicability of the RT-CB from sparse to dense discrete random media
- The results compare favorably to those from the asymptotically exact Superposition *T*-matrix method

Correspondence to:
K. Muinonen,
karri.muinonen@helsinki.fi

Citation:
Muinonen, K., Markkanen, J., Väisänen, T., Peltoniemi, J. I., & Penttilä, A. (2017). Multiple scattering in discrete random media using first-order incoherent interactions. *Radio Science*, *52*, 1419–1431. https://doi.org/10.1002/2017RS006419

Received 25 JUL 2017
Accepted 19 OCT 2017
Accepted article online 27 OCT 2017
Published online 20 NOV 2017

Abstract We consider scattering of electromagnetic waves by a finite discrete random medium composed of spherical particles. The size of the random medium can range from microscopic sizes of a few wavelengths to macroscopic sizes approaching infinity. The size of the particles is assumed to be of the order of the wavelength. We extend the numerical Monte Carlo method of radiative transfer and coherent backscattering (RT-CB) to the case of dense packing of particles. We adopt the ensemble-averaged first-order incoherent extinction, scattering, and absorption characteristics of a volume element of particles as input for the RT-CB. The volume element must be larger than the wavelength but smaller than the mean-free path length of incoherent extinction. In the radiative transfer part, at each absorption and scattering process, we account for absorption with the help of the single-scattering albedo and peel off the Stokes parameters of radiation emerging from the medium in predefined scattering angles. We then generate a new scattering direction using the joint probability density for the local polar and azimuthal scattering angles. In the coherent backscattering part, we utilize amplitude scattering matrices along the radiative-transfer path and the reciprocal path and utilize the reciprocity of electromagnetic waves to verify the computation. We illustrate the incoherent volume element scattering characteristics and compare the dense-medium RT-CB to asymptotically exact results computed using the Superposition *T*-matrix method (STMM). We show that the dense-medium RT-CB compares favorably to the STMM for the current cases of sparse and dense discrete random media studied.

1. Introduction

Multiple electromagnetic scattering in discrete random media of particles constitutes a challenging computational problem in classical electromagnetics. Whereas wavelength-scale random media can be assessed accurately using, for example, the Superposition *T*-Matrix (STMM; e.g., Mackowski & Mishchenko, 2011; Markkanen & Yuffa, 2017) and volume integral equation methods (e.g., Ylä-Oijala et al., 2014), unsurmountable computational difficulties arise for random media much larger than the wavelength. Furthermore, whereas the classical radiative transfer approximation accompanied with coherent backscattering (RT-CB; Muinonen, 2004) has been validated for sparse random media with particle volume densities smaller than ∼5% (Muinonen et al., 2012), no accurate computational methods are available for dense random media with high volume densities.

Our scientific motivation for resolving the open computational problem derives from two ubiquitous astrophysical phenomena observed at small solar phase angles (the Sun-Object-Observer angle) for the Moon, asteroids, Saturn's rings, transneptunian objects, and atmosphereless solar system objects at large. First, a nonlinear increase of brightness, commonly called *the opposition effect* (e.g., Barabashev, 1922), is observed toward the zero phase angle in the magnitude scale. Second, the scattered light is observed to be partially linearly polarized parallel to the Sun-Object-Observer plane, commonly called *negative polarization* (Lyot, 1929). This is contrary to the common positive polarization perpendicular to the scattering plane arising from Rayleigh scattering and Fresnel reflection. In 1980s, the coherent backscattering mechanism was suggested as a partial explanation for the phenomena (Muinonen, 1989; Shkuratov, 1985).

The RT-CB Monte Carlo ray tracing method relies on exponential extinction in a homogeneous scattering and absorbing medium, where the scatterers are assumed to be in each others' far-field regimes. Multiple scattering takes place in the far-field approximation and is fully described by the 2×2 Jones scattering amplitude matrices for the incident, fully transversely polarized electromagnetic field. The field representation

is required due to the tracing of the electromagnetic phase difference between wave components interacting along reciprocal paths. The 4×4 Mueller scattering matrices are utilized, for example, in the generation of new interaction directions and in the numerical integration of the radiative transfer-only (RT-only) signal.

We generalize the RT-CB for dense discrete random media of scattering and absorbing particles by introducing incoherent first-order interactions among volume elements of particles within the random media (for an early approach, see Muinonen, Markkanen, Penttilä, Väisänen, et al., 2016; Muinonen, Markkanen, Penttilä, Virkki, et al., 2016). In the first-order approximation, the scattered field of a given volume element realization is the sum of the fields due to the individual spherical particles, accounting for the electromagnetic phase of the incident field as well as the phase originally due to Green's function. In size, the volume elements must be of the order of the wavelength or larger but nevertheless smaller than the extinction mean-free path of the medium. The discrete random medium is considered to be fully packed with the volume elements, that is, the volume density of the elements is 100%.

Our approach has been triggered, first, by the earlier Monte Carlo studies on volume element extinction in random media of particles with sizes near and within the Rayleigh regime (Lu et al., 1995; Zurk et al., 1995). Second, earlier studies mostly based on the Percus-Yevick approximation (e.g., Tsang et al., 1985; Tsang & Ishimaru, 1987) as well as the more recent derivation of the RT equation from the Maxwell equations for sparse discrete random media (Mishchenko et al., 2006) have encouraged us to search for more precise RT-related multiple-scattering methods for dense media. In summary, introducing incoherent volume elements promises to remove shortcomings in classical RT for sparse random media.

In section 2, we present the basic theoretical framework for scattering and absorption by spherical particles. We then describe multiple scattering in discrete spherical random media with sizes varying from the length scale of a few wavelengths upward. We introduce the incoherent extinction, scattering, and absorption coefficients of a volume element of particles. Section 3 provides an assessment of the numerical methods for the computation of the extinction, scattering, and absorption coefficients, as well as the incoherent scattering matrix elements. We also describe the key points of the Monte Carlo RT-CB method. In section 4, we show our first results for incoherent volume element scattering characteristics and compare the results to those obtained using the STMM. In section 5, we close the work with conclusions and future prospects.

2. Scattering Theory

2.1. Spherical Particles

Consider incident electromagnetic plane wave field in free space with wavelength λ and wave number $k = 2\pi/\lambda$. For a spherical particle with size parameter $x = ka$ (a is radius) and complex refractive index m isolated in free space, the extinction, scattering, and absorption cross sections (respectively $\sigma_{\rm e}$, $\sigma_{\rm s}$, and $\sigma_{\rm a}$) and efficiencies ($q_{\rm e}$, $q_{\rm s}$, and $q_{\rm a}$) are (Bohren & Huffman, 1983)

$$\begin{aligned} q_{\rm e} &= \frac{\sigma_{\rm e}}{\pi a^2} = \frac{2}{x^2}\sum_{l=1}^{\infty}(2l+1)\mathrm{Re}(a_l + b_l), \\ q_{\rm s} &= \frac{\sigma_{\rm s}}{\pi a^2} = \frac{2}{x^2}\sum_{l=1}^{\infty}(2l+1)(|a_l|^2 + |b_l|^2), \\ q_{\rm a} &= \frac{\sigma_{\rm a}}{\pi a^2} = q_{\rm e} - q_{\rm s}. \end{aligned} \tag{1}$$

Here a_l and b_l are the vector spherical harmonics coefficients of the scattered electromagnetic field:

$$\begin{aligned} a_l &= \frac{m\psi_l(mx)\psi_l'(x) - \psi_l(x)\psi_l'(mx)}{m\psi_l(mx)\xi_l'(x) - \xi_l(x)\psi_l'(mx)}, \\ b_l &= \frac{\psi_l(mx)\psi_l'(x) - m\psi_l(x)\psi_l'(mx)}{\psi_l(mx)\xi_l'(x) - m\xi_l(x)\psi_l'(mx)}, \end{aligned} \tag{2}$$

where ψ_l and ξ_l are Riccati-Bessel functions and strictly related to the spherical Bessel and Hankel functions j_l and $h_l^{(1)}$,

$$\begin{aligned} \psi_l(x) &= x j_l(x), \\ \xi_l(x) &= x h_l^{(1)}(x). \end{aligned} \tag{3}$$

The single-scattering albedo is

$$\tilde{\omega} = \frac{q_s}{q_e} = \frac{\sigma_s}{\sigma_e}. \tag{4}$$

The scattering matrix $\mathbf{S}^{LM}$ and the normalized scattering phase matrix $\mathbf{P}^{LM}$ for spherical particles are (superscript LM for Lorenz-Mie)

$$\begin{aligned}
\mathbf{S}^{LM} &= \frac{k^2\sigma_s}{4\pi}\mathbf{P}^{LM}, \\
\mathbf{P}^{LM} &= \frac{2}{x^2 q_s}\begin{pmatrix} |S_{\parallel\parallel}|^2 + |S_{\perp\perp}|^2 & |S_{\parallel\parallel}|^2 - |S_{\perp\perp}|^2 & 0 & 0 \\ |S_{\parallel\parallel}|^2 - |S_{\perp\perp}|^2 & |S_{\parallel\parallel}|^2 + |S_{\perp\perp}|^2 & 0 & 0 \\ 0 & 0 & \mathrm{Re}(S^*_{\perp\perp}S_{\parallel\parallel}) & \mathrm{Im}(S^*_{\perp\perp}S_{\parallel\parallel}) \\ 0 & 0 & -\mathrm{Im}(S^*_{\perp\perp}S_{\parallel\parallel}) & \mathrm{Re}(S^*_{\perp\perp}S_{\parallel\parallel}) \end{pmatrix}, \\
\int_{4\pi} \frac{d\Omega}{4\pi} P_{11}^{LM}(\Omega) &= 1,
\end{aligned} \tag{5}$$

where the amplitude scattering matrix elements $S_{\perp\perp}$ and $S_{\parallel\parallel}$ are

$$\begin{aligned}
S_{\perp\perp} &= \sum_{l=1}^{\infty} \frac{2l+1}{l(l+1)} \left[a_l \frac{dP_l^1(\cos\theta)}{d\theta} + b_l \frac{1}{\sin\theta} P_l^1(\cos\theta) \right], \\
S_{\parallel\parallel} &= \sum_{l=1}^{\infty} \frac{2l+1}{l(l+1)} \left[a_l \frac{1}{\sin\theta} P_l^1(\cos\theta) + b_l \frac{dP_l^1(\cos\theta)}{d\theta} \right],
\end{aligned} \tag{6}$$

and P_l^1 are associated Legendre functions.

2.2. Superposition *T*-Matrix Method

Consider electromagnetic scattering by a system of multiple nonintersecting spheres in the frequency domain using the Maxwell equations. The scattering problem can be solved by applying the superposition principle, that is, the total scattered field $\mathbf{E}^s$ can be represented as the sum of partially scattered fields $\mathbf{E}_i^s$ from each sphere:

$$\mathbf{E}^s = \sum_{i=1}^{N} \mathbf{E}_i^s, \tag{7}$$

in which N is the number of spheres. The partial fields are expanded with the spherical vector wave functions $\mathbf{M}_\nu$ expressed with respect to the origin of the ith sphere as

$$\mathbf{E}_i^s \approx \sum_{\nu} a_i^\nu \mathbf{M}_\nu, \tag{8}$$

where a_i are the scattering coefficients and ν is the multiindex $\nu = \{n, m, k\}$ with $n = 1, \ldots, N,\ m = -n, \ldots, n$, and $k = 1, 2$. The scattering equations in coefficient space can be expressed as

$$a_i^{sca} = T_i a_i^{inc} + T_i \sum_{j=1, j\neq i}^{N} (S|R)_i^j a_j^{sca} \quad \text{for all } i = 1, \ldots, N, \tag{9}$$

where T_i is the T-matrix of the ith sphere and $(S|R)_i^j$ is the translation matrix that translates the coefficients a_j^{sca} of the scattered field by sphere j into the incoming coefficients of sphere i (Cruzan, 1962).

The scattering equation (9) is solved iteratively by the generalized minimum residual method. The matrix-vector multiplication, required in each iteration step, is accelerated by the fast multipole method (Greengard & Rokhlin, 1987; Gumerov & Duraiswami, 2005). In our implementation (FaSTMM, Markkanen & Yuffa, 2017), the so-called rotation → axial translation → inverse rotation technique is used with recursive computations of the axial translation (Chew, 1992) and rotation coefficients (Choi et al., 1999).

2.3. Scattering by Discrete Random Media

Consider next a finite, spherical medium (radius R, size parameter $X = kR$) of randomly distributed spherical particles with a volume density of v (Figure 1). The finite medium is assumed to be located in free space, and an RT-CB solution is searched for the extinction, scattering, and absorption characteristics of the medium. It is here postulated that the incoherent extinction, scattering, and absorption characteristics for a volume element of the medium are needed as input for the numerical method.

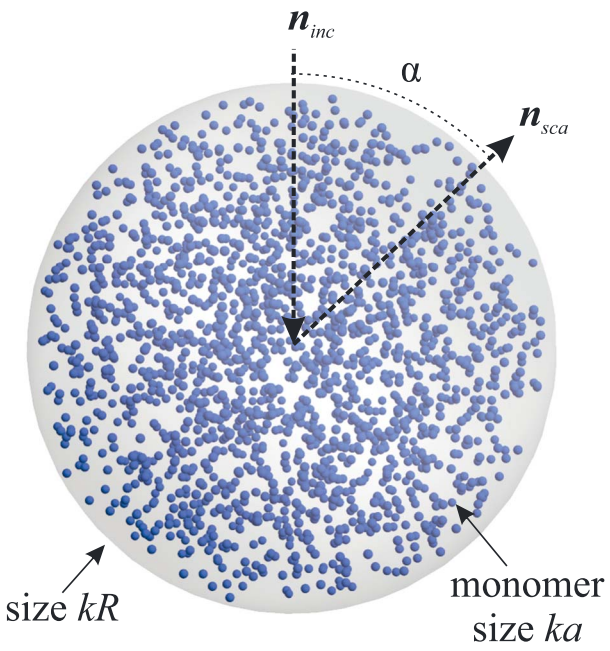

Figure 1. Discrete spherical random medium of equal-sized spherical particles. The phase angle α denotes the angle between the source of illumination (in the direction $-\mathbf{n}_{\rm inc}$) and the observer ($\mathbf{n}_{\rm sca}$) as seen from the object. The scattering angle is $\theta = \pi - \alpha$. The size parameters of the random medium and particles are kR and ka, respectively. Finally, $k = 2\pi/\lambda$ is the wave number and λ is the wavelength.

In order to proceed, we utilize the spherical geometry once more: consider a spherical volume element (radius R_0, size parameter $X_0 = kR_0$) completely within the random medium. We assign a spherical particle to the volume element if the particle center is located within the element. We envisage that the volume density is approximately balanced by the omission of particles intersecting the volume element but with their centers nevertheless outside the volume element. Furthermore, for the time being, we omit any surface effects arising from the volume element intersecting the boundary of the random medium.

Due to the stochastic nature of the random medium, the number and location of the spherical particles within the volume element will vary both as a function of the element location in the random medium realization and from one random medium realization to another.

Let us derive the ensemble-averaged incoherent extinction, scattering, and absorption coefficients of the volume element. We write the ensemble-averaged first moment of the field scattered by the volume element (the mean or coherent scattered field) as

$$\mathbf{E}^{\rm s,c}(\mathbf{r}) = \langle \mathbf{E}^{\rm s}(\mathbf{r}) \rangle = \lim_{n\to\infty} \frac{1}{n} \sum_{i=1}^{n} \mathbf{E}_i^{\rm s}(\mathbf{r}), \tag{10}$$

where n is the number of volume element realizations and $\mathbf{E}_i^{\rm s}$ is the scattered field from volume element realization i.

The incoherent scattered field from volume element realization i is then obtained by subtracting the coherent scattered field from the scattered field of the realization,

$$\mathbf{E}_i^{\rm s,ic}(\mathbf{r}) = \mathbf{E}_i^{\rm s}(\mathbf{r}) - \mathbf{E}^{\rm s,c}(\mathbf{r}). \tag{11}$$

Consequently, the first moment of the incoherent scattered field vanishes,

$$\langle \mathbf{E}^{\rm s,ic}(\mathbf{r}) \rangle \equiv 0, \tag{12}$$

and the second moment of the incoherent scattered field equals

$$\langle |\mathbf{E}^{\rm s,ic}(\mathbf{r})|^2 \rangle = \langle |\mathbf{E}^{\rm s}(\mathbf{r})|^2 \rangle - |\mathbf{E}^{\rm s,c}(\mathbf{r})|^2. \tag{13}$$

Within the present framework, the second moment of the scattered field thus equals the sum of the second moment of the incoherent field and the absolute value of the coherent field squared.

In the first-order approximation, the scattered far field of volume element realization i at distance r is the sum of the free space scattered fields of the N_i identical spherical particles with scattering amplitude $\mathbf{A}^{\rm s}$ located at $\mathbf{r}_j$ ($j = 1, \ldots, N_i$)

$$\begin{aligned} \mathbf{E}_i^{\rm s}(\mathbf{r}) &= \sum_{j=1}^{N_i} \mathbf{E}_{ij}^{\rm s}(\mathbf{r}_j) = \frac{\exp(ikr)}{-ikr} \mathbf{A}^{\rm s} \sum_{j=1}^{N_i} \exp(i\mathbf{q}\cdot\mathbf{r}_j), \\ \mathbf{q} &= \mathbf{k}^{\rm i} - \mathbf{k}^{\rm s}, \end{aligned} \tag{14}$$

where $\mathbf{k}^{\rm i} = k\mathbf{e}_z$ and $\mathbf{k}^{\rm s}$ denote the wave vectors of the incident and scattered fields, respectively.

The coherent scattered far field is thus the ensemble average

$$\mathbf{E}^{\rm s,c}(\mathbf{r}) = \frac{\exp(ikr)}{-ikr} \mathbf{A}^{\rm s} \lim_{n\to\infty} \frac{1}{n} \sum_{i=1}^{n} \sum_{j=1}^{N_i} \exp\left(i\mathbf{q}\cdot\mathbf{r}_j^{(i)}\right), \tag{15}$$

where $\mathbf{r}_j^{(i)}$ denotes the location of particle j for the realization i. The incoherent far field of a single realization follows from equations (11), (14), and (15).

We can improve the convergence of ensemble averaging with the help of analytical averaging over orientations. For the coherent scattered field, instead of averaging as in equation (15), we average as follows:

$$\mathbf{E}^{\mathrm{s,c}}(\mathbf{r}) = \frac{\exp(\mathrm{i}kr)}{-\mathrm{i}kr}\mathbf{A}^{\mathrm{s}} \lim_{n\to\infty} \frac{1}{n}\sum_{i=1}^{n}\sum_{j=1}^{N_i} \frac{\sin qr_j^{(i)}}{qr_j^{(i)}}, \qquad q = |\mathbf{q}| = 2k\sin\frac{1}{2}\theta. \tag{16}$$

Similarly, for the squared scattered far field, we obtain (Debye, 1915; see also the Rayleigh-Gans treatment in Muinonen, 1996)

$$|\mathbf{E}^{\mathrm{s}}(\mathbf{r})|^2 = \frac{1}{k^2r^2}\left|\mathbf{A}^{\mathrm{s}}\right|^2 \lim_{n\to\infty}\frac{1}{n}\sum_{i=1}^{n}\sum_{j=1}^{N_i}\sum_{k=1}^{N_i}\frac{\sin q|\mathbf{r}_j^{(i)}-\mathbf{r}_k^{(i)}|}{q|\mathbf{r}_j^{(i)}-\mathbf{r}_k^{(i)}|}. \tag{17}$$

It now follows that the ensemble-averaged incoherent scattering matrix of the volume element is a pure Mueller matrix obtained by multiplying the Mie scattering matrix in equation (5) by a function $H(\theta)$,

$$\begin{aligned} \mathbf{S}_0^{\mathrm{ic}}(\theta) &= H(\theta)\mathbf{S}^{\mathrm{LM}}(\theta), \\ H(\theta) &= F(\theta) - G(\theta), \\ F(\theta) &= \lim_{n\to\infty}\frac{1}{n}\sum_{i=1}^{n}\sum_{j=1}^{N_i}\sum_{k=1}^{N_i}\frac{\sin q|\mathbf{r}_j^{(i)}-\mathbf{r}_k^{(i)}|}{q|\mathbf{r}_j^{(i)}-\mathbf{r}_k^{(i)}|}, \\ G(\theta) &= \left|\lim_{n\to\infty}\frac{1}{n}\sum_{i=1}^{n}\sum_{j=1}^{N_i}\frac{\sin qr_j^{(i)}}{qr_j^{(i)}}\right|^2, \end{aligned} \tag{18}$$

where $F(\theta)$ is the well-known form factor. Furthermore, we can assign a diagonal incoherent amplitude scattering matrix for the volume element,

$$\begin{aligned} S_{\perp\perp,0}^{\mathrm{ic}}(\theta) &= \sqrt{H(\theta)}S_{\perp\perp}(\theta), \\ S_{\parallel\parallel,0}^{\mathrm{ic}}((\theta) &= \sqrt{H(\theta)}S_{\parallel\parallel}(\theta). \end{aligned} \tag{19}$$

The ensemble-averaged incoherent scattering cross section of the volume element results from

$$\sigma_{\mathrm{s},0}^{\mathrm{ic}} = \frac{1}{k^2r^2}\int_{4\pi}\mathrm{d}\Omega\, S_{0,11}^{\mathrm{ic}}(\theta), \tag{20}$$

and, consequently, the incoherent scattering coefficient is

$$\kappa_{\mathrm{s}}^{\mathrm{ic}} = \frac{\sigma_{\mathrm{s},0}^{\mathrm{ic}}}{V_0}, V_0 = \frac{4\pi}{3}R_0^3. \tag{21}$$

The incoherent absorption cross section of the volume element as well as the incoherent absorption coefficient follow from the absorption cross section of the spherical particle

$$\sigma_{\mathrm{a},0}^{\mathrm{ic}}\langle N\rangle\sigma_a, \qquad \kappa_{\mathrm{a}}^{\mathrm{ic}} = \frac{\sigma_{\mathrm{a},0}^{\mathrm{ic}}}{V_0}. \tag{22}$$

The incoherent extinction cross section and coefficient are

$$\sigma_{\mathrm{e},0}^{\mathrm{ic}} = \sigma_{\mathrm{s},0}^{\mathrm{ic}} + \sigma_{\mathrm{a},0}^{\mathrm{ic}}, \qquad \kappa_{\mathrm{e}}^{\mathrm{ic}} = \frac{\sigma_{\mathrm{e},0}^{\mathrm{ic}}}{V_0}, \tag{23}$$

and the mean-free extinction path length is

$$\ell = \frac{1}{\kappa_{\mathrm{e,\,ic}}}. \tag{24}$$

Finally, the single-scattering albedo of the volume element equals

$$\tilde{\omega}^{\mathrm{ic}} = \frac{\sigma_{\mathrm{s},0}^{\mathrm{ic}}}{\sigma_{\mathrm{e},0}^{\mathrm{ic}}}. \tag{25}$$

As for the scattering and absorption characteristics of the discrete random medium, we denote the scattering phase matrix by **P** and the spherical albedo equaling the incoherent single-scattering albedo by A_S.

3. Numerical Methods

3.1. Average Volume Element Characteristics

The volume element scattering, absorption, and extinction characteristics are computed with the help of ensemble averaging over realizations of randomly distributed spherical particles in a predefined volume element. We generate the sample volume elements as follows. First, we draw the number of particles from the Poisson distribution with the help of the mean number of particles $N_0 = vX_0^3/x^3$ in the volume element. Second, we place the spherical volume element in the center of a cubic cell that is the unit cell of a periodically continued random medium of particles. The edge length of the cubic cell is taken to be large enough (with mean number of particles $>16N_0$) so that no artificial disturbances follow for the particle distribution within the spherical volume element. Third, we generate particles within the cubic cell until the given number of particles are obtained within the spherical volume element. Fourth, it is clear that the number of particles in a spherical volume element containing finite-sized particles does not obey the Poisson distribution. At the final stage, we repeat the aforedescribed procedure with a realistic particle-number variance that we describe later in this section.

Consider next the convergence characteristics of ensemble averaging for the functions $F(\theta)$ and $G(\theta)$ in equation (18). The convergence depends strongly on the scattering angle. This is due to the phase factor $\exp(i\mathbf{q}\cdot\mathbf{r})$, where $q = |\mathbf{q}| = 2k\sin\frac{1}{2}\theta$ varies strongly with the scattering angle. For each scattering angle, we face averaging with a specific apparent wavelength $\lambda/(2\sin\frac{1}{2}\theta)$. This apparent wavelength obtains the value of $\lambda/2$ in the exact backscattering direction $\theta = 180^\circ$, rising to λ at $\theta = 60^\circ$, further to 10λ at $\theta \approx 5.73^\circ$, and reaching infinity in the exact forward scattering direction.

It is thus to be expected that, in the backscattering hemisphere, sufficiently accurate results are obtained for small spherical volume elements from size parameters of roughly $kR_0 = 10$ upward. On the contrary, for $\theta = 15^\circ$, even $kR_0 = 40$ does not always suffice. Clearly, a violation of the requirement that the volume element size must be smaller than the mean-free path length of incoherent extinction can easily result. In the forward scattering direction, the results nevertheless follow analytically, since the phase factors reduce to unity.

If the incoherent extinction, scattering, and absorption characteristics were independent of the volume element size, we would be able to move forward to the actual RT-CB computations. There are, however, significant differences in the scattering coefficients as well as the scattering matrix element S_{11} obtained using different volume elements. The differences arise from the challenges in the forward scattering hemisphere described above.

In order to obtain unambiguous incoherent input characteristics for the RT-CB code, we proceed as follows. First, we start by defining the size parameters of the spherical particle and the spherical volume element x and X_0, as well as the volume density of particles v. Second, we generate sample volume elements of spherical particles as described above. Third, we compute and store the scattered far field and its absolute value squared from the spherical volume of particles. Here we speed up the convergence with the help of analytical averaging over orientation for both the scattered far field and its value squared. Fourth, we repeat the aforedescribed steps for a large number of realizations of spherical volumes of particles. Fifth, we repeat the entire computation for a number of volume element size parameters, typically $X_0 = 10$, 15, 20, and 40.

Finally, we repeat the entire analysis iteratively with a particle-number variance lowered from the nominal Poisson value until smooth and convergent, maximally invariant incoherent characteristics are obtained for the volume elements near the forward scattering direction. This is a regularization procedure, and the true numbers of particles in the volume elements of an infinite discrete random medium do not necessarily conform to the statistics imposed here. The procedure allows us to define extinction, scattering, and absorption characteristics as per volume on a range of sizes slightly above the wavelength scale. The procedure further underscores how critically important is the actual number distribution of particles in the volume element.

3.2. Radiative Transfer Coherent Backscattering Method

The RT-CB method has been developed originally for homogeneous, finite, and semiinfinite plane-parallel media of spherical scatterers (Muinonen, 2004). In what follows, we focus on the RT-CB computation

in a spherical discrete random medium filled with scatterers (Muinonen et al., 2012; Muinonen & Videen, 2012; Videen & Muinonen, 2015). The spherical geometry is attractive due to several reasons. For example, it has allowed Videen and Muinonen (2015) to study light-scattering evolution from single particles to a regolith by gradually increasing the size of the medium toward macroscopic scales. For another example, it has allowed detailed comparisons between the RT-CB method and the STMM method (Muinonen et al., 2012).

An essential feature of the numerical RT-CB technique is the a priori selection of scattering directions for updating Stokes parameters during the Monte Carlo radiative transfer computation, thus avoiding the collection of rays into finite bins. Fixed angles allow for the computation of electromagnetic phase differences and thus the coherent backscattering effect. In the technique, there are two sets of fixed angles. First, the radiative transfer set utilizes Gauss-Legendre abscissae and weights for the phase angle (Press et al., 1992) and uniform spacing for the azimuthal angle. Second, the radiative transfer coherent backscattering set can be chosen to cover any angular domain desired.

For the RT-CB set, the following angular scheme is incorporated. The azimuthal angle is uniformly spaced with eight angles: in general, the number must be a multiple of eight in order for the azimuthal angle grid to be utilized in the symmetry relations making the computation efficient. The phase angle (or backscattering angle) currently takes on 51 values between $\alpha = 0.0°$ and $\alpha = 180.0°$ with a concentration of angles near the backscattering direction.

In the generation of new interaction directions, the scattering angle is generated by using the cumulative distribution function based on the Mueller element $P^{\mathrm{ic}}_{0,11}$. Then the Kepler equation is solved using the Newton method for the azimuthal scattering angle. Within the media, due to constant updating of the Stokes parameters of scattered light, the generation of directions is coupled with the generation of the path lengths, confining the subsequent scattering processes into the scattering medium.

Since the original numerical method (Muinonen, 2004), three main changes have been introduced to make the method more robust and accurate (Muinonen & Videen, 2012; Videen & Muinonen, 2015). First, whereas the original method makes use of the reciprocity relation of electromagnetic scattering in the computation of the coherent backscattering contribution in the exact backscattering direction, the present method utilizes scattering amplitude matrices directly and allows for the reciprocity relation to be used as a measure of computational accuracy.

Second, symmetry relations are utilized to improve the numerical convergence of the angular scattering patterns, in particular, in the case of spherical media. There are six incident polarization states that need to be traced in order to obtain the corresponding contributions to the scattering matrix of the spherical medium. In the optimized method, one Markov chain of scatterings is computed in the case of linear polarization and another one in the case of circular polarization. The three remaining linear polarization chains follow, after proper mapping, from the one computed. Analogously, the one remaining circular polarization chain follows from the one computed. The improvement of the convergence is substantial, and the numerical results have been verified against those from the original method.

Third, the finite size of the volume element is accounted for probabilistically. When interaction distances smaller than the volume element diameter are generated, that is, when the current and the trial next volume element appear to overlap, we draw a uniform random deviate within $u \in]0, 1[$ and reject the interaction distance if

$$u < \frac{\Delta V}{V_0}, \tag{26}$$

where ΔV denotes intersectional volume of the two elements. In the case of rejection, we repeat the generation of the distance (together with the direction).

4. First Results With Discussion

In what follows, we will compare RT-CB results with those obtained by using the Superposition T-matrix method (Markkanen & Yuffa, 2017; Mackowski & Mishchenko, 2011) for a spherical medium (Figure 1) with size parameter $X = kR = 40$ with varying volume density v. For the STMM method, the sample discrete media have been generated using Poisson statistics with the mean number of particles also describing the variance in the number of particles. We point out that, with the RT-CB comparison in mind, what actual distribution one should incorporate for the STMM computations is a nontrivial question.

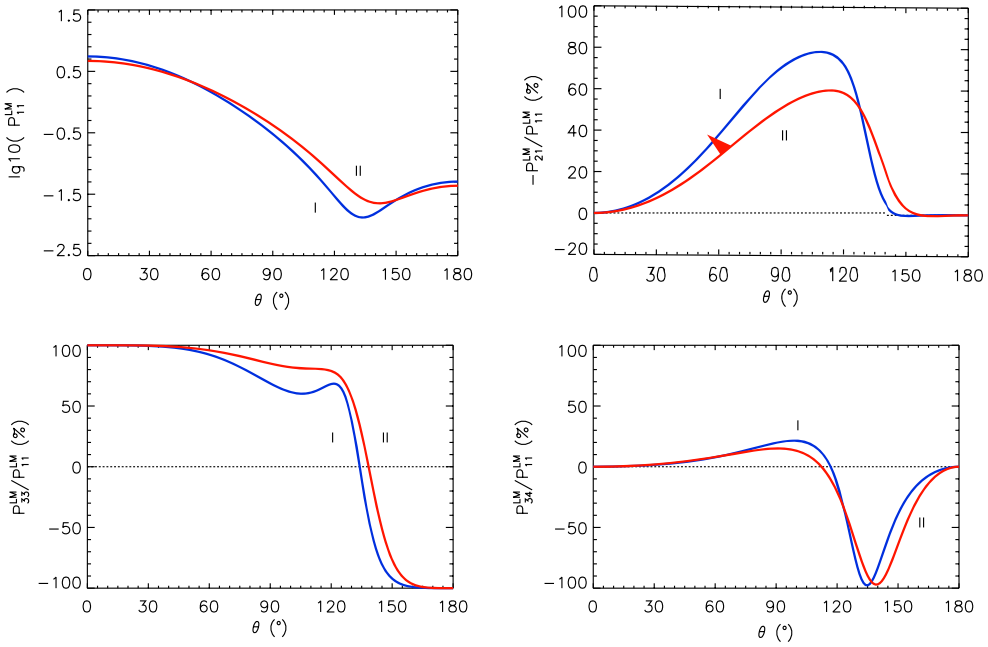

Figure 2. Lorenz-Mie scattering phase matrix elements (top left) P_{11}^{LM}, (top right) $-P_{21}^{\mathrm{LM}}/P_{11}^{\mathrm{LM}}$, (bottom left) $P_{33}^{\mathrm{LM}}/P_{11}^{\mathrm{LM}}$, and (bottom right) $P_{34}^{\mathrm{LM}}/P_{11}^{\mathrm{LM}}$ as a function of the scattering angle θ for the ice (blue line, Case I) and silicate cases (red line, Case II): Case I, size parameter $x = 2$, refractive index $m = 1.31$. Case II: $x = 1.76$, $m = 1.50$.

In terms of composition, we consider two cases of discrete random media composed of equal-sized, nonabsorbing spherical particles. In the first case (ice, Case I), the size parameter is $x = 2$ and the refractive index is $m = 1.31$. In the second case (silicate, Case II), the size parameter is $x = 1.76$ and the refractive index is $m = 1.50$. Figure 2 shows the scattering phase matrix elements for the two spherical particles as a function

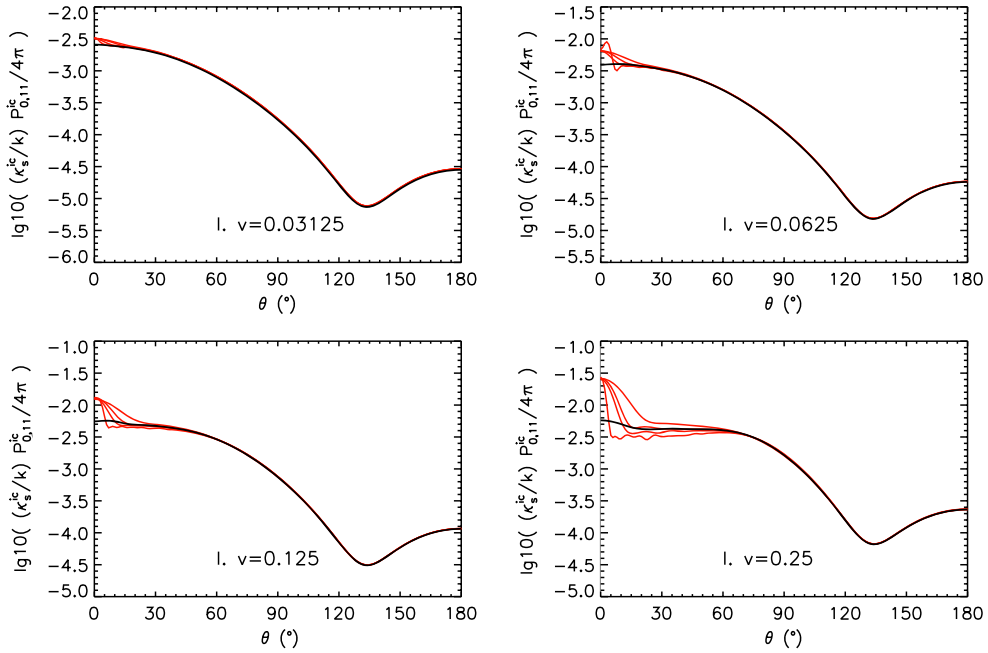

Figure 3. Volume element incoherent scattering phase matrix element $P_{0,11}^{\mathrm{ic}}$ (scattering phase function) for Case I (ice) for varying volume elements (thin red lines) as a function of the scattering angle. The phase function has been normalized to yield the incoherent scattering coefficient κ_s^{ic}/k upon integration over the solid angle. Also depicted is the final phase function (thick black line) obtained by regularizing the variance for the number of particles.

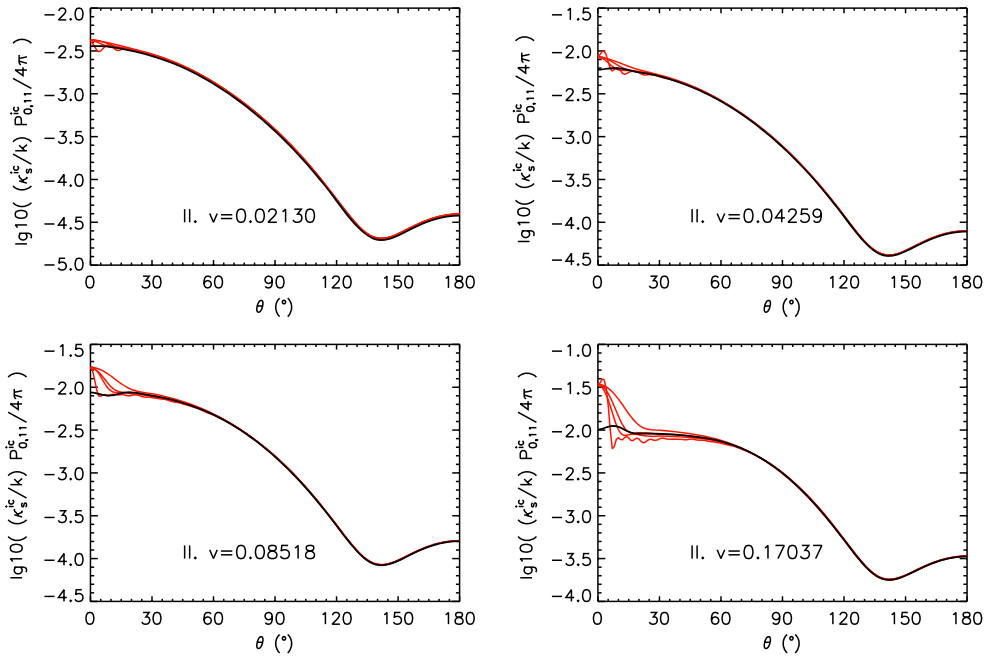

Figure 4. As in Figure 3 for Case II (silicate).

of the scattering angle. These specific kinds of particles have been studied earlier in, for example, Muinonen et al. (2012), in the context of coherent backscattering by sparse discrete random media. In particular, there is no significant negative polarization in either case (Figure 2).

We now compute the incoherent volume element extinction, scattering, and absorption characteristics. As we consider nonabsorbing particles, we are merely concerned with the scattering characteristics, and the incoherent extinction and scattering coefficients coincide. Figures 3 and 4 illustrate the incoherent volume element scattering phase matrix element $P^{\rm ic}_{0,11}$ as a function of volume element size parameter, normalized so as to yield the incoherent scattering coefficient $\kappa^{\rm ic}_s/k$ upon integration over the full solid angle. Notice that the other matrix elements, expressed as ratios $P^{\rm ic}_{0,ij}/P^{\rm ic}_{0,11}$, equal those illustrated in Figure 2 for the spherical particles.

We have repeated the computation of $(\kappa^{\rm ic}_s/k)P^{\rm ic}_{0,11}/(4\pi)$ for the size parameters $X_0 = kR_0 = 10$, 15, 20, and 40 for altogether eight volume densities. For Case I, we assume that $v = 3.125\%$, 6.25%, 12.5%, or 25%, corresponding to the mean number of particles of 250, 500, 1,000, and 2,000, respectively. For Case II, we assume the same mean number of particles, resulting in the volume densities $v = 2.130\%$, 4.259%, 8.518%, or 17.037%. In comparison to our earlier study (Muinonen et al., 2012), we have thus added the cases of 1,000 and 2,000 particles, raising the volume density clearly beyond the validity domain of classical radiative transfer.

Figures 3 and 4 show, first, that the normalized phase functions are in excellent agreement across a wide range of scattering angles from the backscattering hemisphere toward forward scattering. Second, they show the challenges near the forward scattering direction: a persistent diffraction-like feature appears in all cases. Third, Figures 3 and 4 show that the regularization method relying on downsizing the variance successfully removes the diffraction-like feature. Fourth, for both Cases I and II, the normalized phase function tends to saturate near the forward scattering direction with increasing volume density. Simultaneously, the phase function tends to rise near the backward scattering direction. In conclusion, we can utilize an unambiguous volume element incoherent scattering phase matrix in RT-CB computations. In detail, we have derived this scattering phase matrix using $X_0 = 15$ and downsizing the variance with the help of the first-round result using $X_0 = 20$ (enforcing the forward direction value to be equal to the first-round result at $\theta = 10°$).

With the incoherent input parameters in order, we can turn to the RT-CB computation for the discrete spherical random media of spherical particles. Figures 5 and 6 show the results for Cases I and II, and certain key numbers are collected in Table 1. For sparse media studied earlier by Muinonen et al. (2012) using the RT-CB method

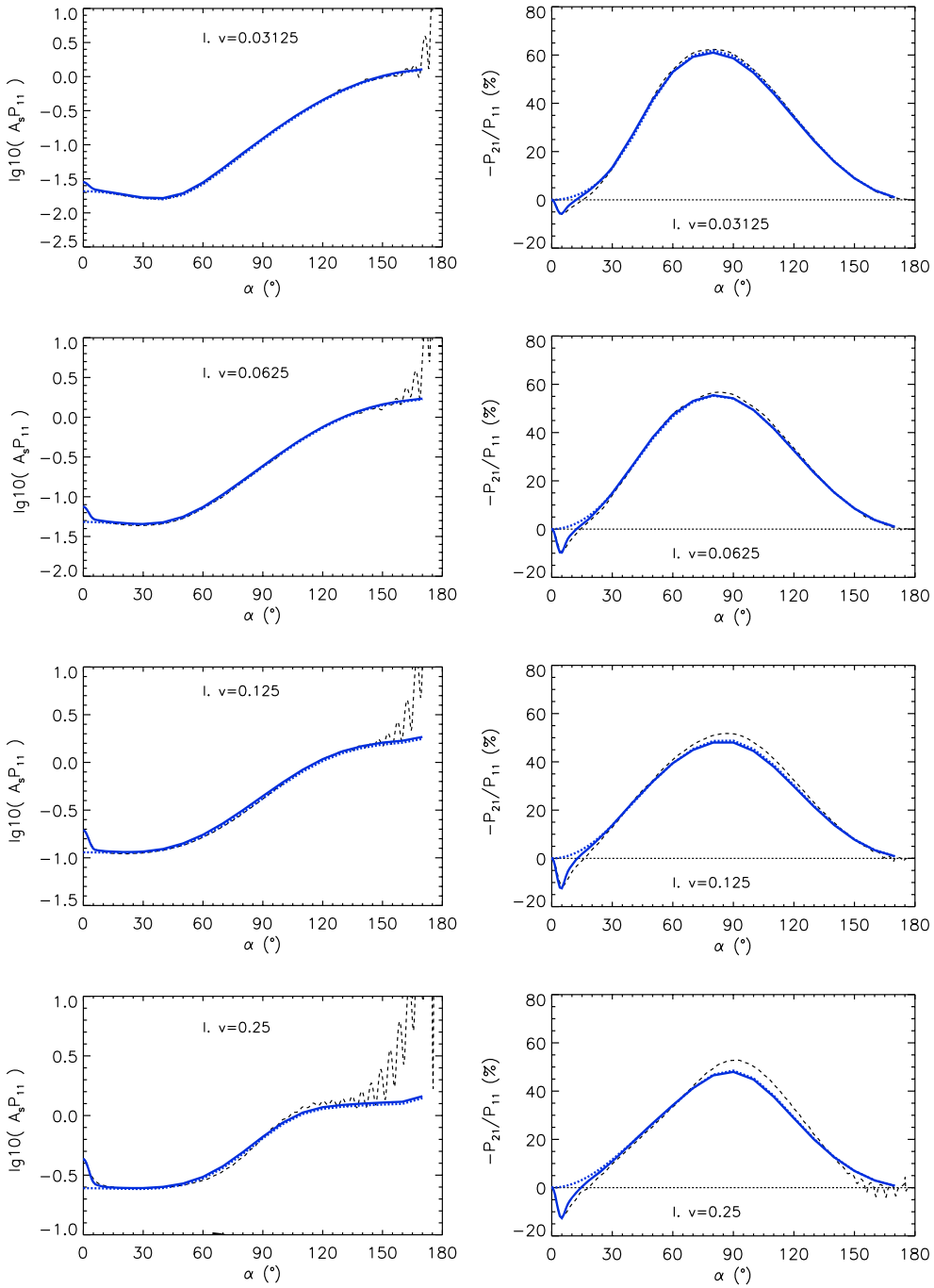

Figure 5. Scattering phase matrix elements $A_S P_{11}$ and $-P_{21}/P_{11}$ for spherical discrete random media (size parameter $kR = 40$, varying volume density v) of spherical particles as a function of the phase angle α. We show the results for Case I (ice with size parameter $x = 2$ and refractive index $m = 1.31$) as computed using the RT-CB (solid line) and the Superposition T-matrix methods (dashed line). Also shown are the RT-only results (dotted line). A_S denotes the spherical albedo of the random medium, allowing for absolute comparison between the two methods.

with the Lorenz-Mie scattering characteristics as input, the agreement with the STMM results is here even better. We recall that the dense-media RT-CB incorporates a probabilistic treatment for overlapping volume elements, when generating the next interaction point. There is no counterpart in the RT-CB with independent scattering: accounting for the spherical particle size would cause a negligible effect on the angular scattering characteristics.

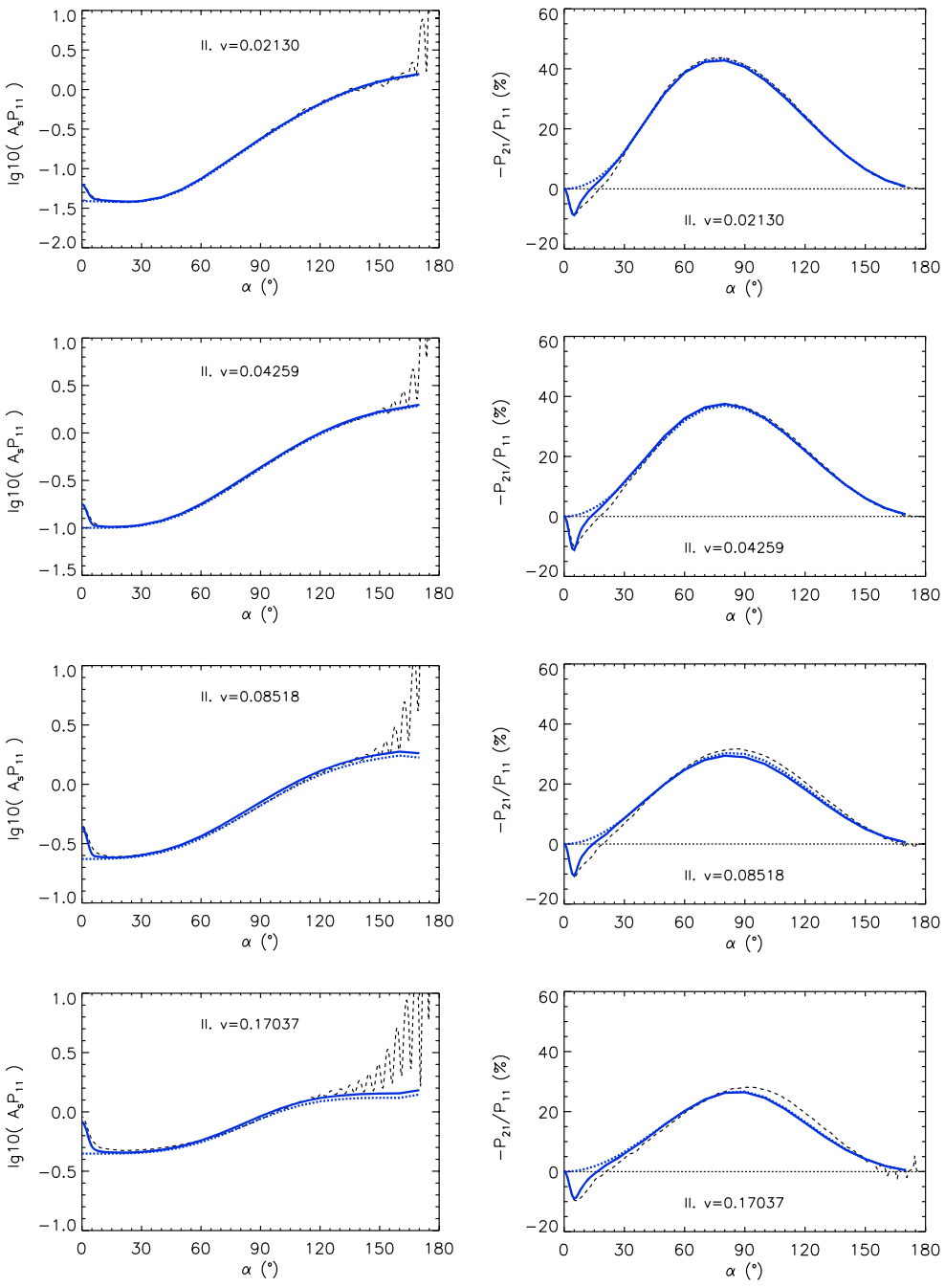

Figure 6. As in Figure 5 for Case II (silicate) with $x = 1.76$ and $m = 1.50$.

For the cases of dense media, the RT-CB with incoherent input characteristics works perhaps surprisingly well, considering that only first-order input is utilized. There are deviations between the RT-CB and STMM results in the negative polarization branch, but these differences may be due to the fact that the discrete medium statistics for generating the STMM results are bound to differ from the corresponding statistics for the RT-CB results. The two most important statistical parameters of the discrete random medium are the mean and variance of the number of particles in the medium.

Table 1 shows the evolution of the incoherent extinction mean-free path length and incoherent extinction coefficient for Cases I and II as a function of the volume density. It also shows how the incoherent

Table 1
The Volume Densities v, Dimensionless Incoherent Scattering Mean-Free Path Lengths $k\ell$ and Coefficients κ_s^{ic}/k, As Well As the Resulting Spherical Albedos A_S, Geometric Albedos p, and Enhancement Factors ζ for the Cases Studied

v	$k\ell$	$\kappa_s^{ic}/k(10^{-2})$	A_S	p (%)	ζ
		Case I, ice			
0.03125	155.80	0.64184	0.29	0.68	1.34
0.06250	83.869	1.1923	0.46	1.79	1.54
0.12500	50.953	1.9626	0.62	4.89	1.70
0.25000	39.487	2.5325	0.71	11.16	1.76
		Case II, silicate			
0.02130	97.726	1.0233	0.41	1.49	1.60
0.04259	51.181	1.9539	0.62	4.49	1.77
0.08518	29.540	3.3852	0.79	11.44	1.85
0.17037	20.128	4.9683	0.88	22.92	1.86

spherical albedo, geometric albedo, and backscattering enhancement factor of the discrete random medium evolve with the volume density. For both cases, the enhancement factor shows saturation toward the highest volume density—the saturation is stronger for the silicate case where the mean-free path lengths are shorter. We note that, for $X_0 = 40$, the volume element size equals the size of the spherical random medium itself. Furthermore, for $X_0 = 40$ in Cases I and II as well as for $X_0 = 20$ in Case II, the volume element size is close to or exceeds the resulting incoherent extinction mean-free path length. In spite of the evident violation against the validity criterions (see section 1), we have included these cases in the analysis, too, as they allow for the formal mapping of the mean-free path length with increasing volume element size.

The first results suggest that there is a collective incoherent polarization effect for phase angles larger than about 90° (Figures 5 and 6, bottom right): there is a tendency for the exact computation to yield more positive polarization than what results from the RT-CB computation. This unknown phenomenon can be due to bisphere resonances similar to those verified for circular polarization in the backscattering direction by Virkki et al. (2015). The phenomenon can also be related to the fact that independent orders of scattering must fail to describe the full scattered field for grazing angles of emergence (see, e.g., Lindell et al., 1991; Muinonen et al., 1991). Studying the ultimate cause for the phenomenon is, however, beyond the scope of the present study.

5. Conclusions

We have studied multiple scattering by finite discrete random media of spherical particles using the radiative transfer coherent backscattering method. By introducing first-order incoherent interaction between the incident field and the volume element, we have successfully extended the RT-CB method to dense random media markedly beyond the validity regime of classical radiative transfer.

There are a number of questions arising on the basis of the present study. First, all the current example computations have concerned nonabsorbing spherical particles with low to moderately high refractive indices. It remains to be studied where the limits of the first-order incoherent treatment exactly are, a task that can be assessed with the help of the Superposition *T*-matrix method. Second, it is our near-term plan to replace the first-order incoherent interaction with a rigorous treatment, again, using *T*-matrices. Finally, we intend to incorporate nonspherical particles and extend the numerical methods accordingly.

Acknowledgments
The research has been supported by the European Research Council with Advanced Grant 320773 SAEMPL, Scattering and Absorption of ElectroMagnetic waves in ParticuLate media. The computational resources have been provided by CSC—IT Centre for Science Ltd, Finland. The open-source computer software utilized for the computation of the numerical data is available from the authors at https://wiki.helsinki.fi/display/PSR/Planetary+System+Research+group.

References

Barabashev, N. P. (1922). Bestimmung der Erdalbedo und des Reflexionsgesetzes für die Oberfläche der Mondmeere. Theorie den Rillen. *Astronomische Nachrichten*, *217*, 445–452.
Bohren, C. F., & Huffman, D. R. (1983). *Absorption and Scattering of Light by Small Particles*. New York: Wiley.
Chew, W. C. (1992). Recurrence relations for three-dimensional scalar addition theorem. *Journal of Electromagnetic Waves and Applications*, *6*, 133–142.
Choi, C. H., Ivanic, J., Gordon, M. S., & Ruedenberg, K. (1999). Rapid and stable determination of rotation matrices between spherical harmonics by direct recursion. *The Journal of Chemical Physics*, *111*, 8825–8831.
Cruzan, O. R. (1962). Translation addition theorems for spherical vector wave function'. *Quarterly of Applied Mathematics*, *20*, 33–40.
Debye, P. (1915). Zerstreuung von Röntgenstrahlen. *Annalen der Physik*, *46*, 809–823.
Greengard, L., & Rokhlin, V. (1987). A fast algorithm for particle simulations. *Journal of Computational Physics*, *73*, 325–348.
Gumerov, N. A., & Duraiswami, R. (2005). Computation of scattering from clusters of spheres using the fast multipole method. *The Journal of the Acoustical Society of America*, *117*, 1744–1761.
Lindell, I. V., Sihvola, A. H., Muinonen, K. O., & Barber, P. W. (1991). Scattering by a small object close to an interface. I: Exact image theory formulation. *Journal of the Optical Society of America A*, *8*, 472–476.
Lu, C. C., Chew, W. C., & Tsang, L. (1995). The application of recursive aggregate T-matrix algorithm in the Monte Carlo simulations of the extinction rate of random distribution of particles. *Radio Science*, *30*(1), 25–28.
Lyot, B. (1929). Recherches sur la polarisation de la lumière des planètes et de quelquessubstances terrestres. *Annales de l'Observatoire de Paris*, *8*(1), 1–161.
Mackowski, D. W., & Mishchenko, M. I. (2011). A multiple sphere T-matrix FORTRAN code for use on parallel computer clusters. *Journal of Quantitative Spectroscopy and Radiative Transfer*, *112*, 2182–2192.
Markkanen, J., & Yuffa, A. J. (2017). Fast superposition T-matrix solution for clusters with arbitrarily-shaped constituent particles. *Journal of Quantitative Spectroscopy and Radiative Transfer*, *189*, 181–189.
Mishchenko, M. I., Travis, L. D., & Lacis, A. A. (2006). *Multiple Scattering of Light by Particles*. Cambridge, UK: Cambridge University Press.
Muinonen, K. (1989). Electromagnetic scattering by two interacting dipoles. In *URSI Electromagnetic Theory Symposium (EMTS'89)* (pp. 428–430). Stockholm, Sweden.

Muinonen, K. (1996). Light scattering by Gaussian random particles: Rayleigh and Rayleigh-Gans approximations. *Journal of Quantitative Spectroscopy and Radiative Transfer*, *55*, 603–613.
Muinonen, K. (2004). Coherent backscattering of light by complex random media of spherical scatterers: Numerical solution. *Waves Random Media*, *14*, 365–388.
Muinonen, K., & Videen, G. (2012). A phenomenological single scatterer for studies of complex particulate media. *Journal of Quantitative Spectroscopy and Radiative Transfer*, *113*, 2385–2390.
Muinonen, K., Markkanen, J., Penttilä, A., Väisänen, T., & Peltoniemi, J. (2016). Multiple scattering by dense random media: Numerical solution. In *Electromagnetic Theory Symposium (EMTS'16)* (pp. 400–403). Espoo, Finland.
Muinonen, K., Markkanen, J., Penttilä, A., Virkki, A., & Mackowski, D. (2016). Multiple scattering by dense random media: Volume-element extinction. In *URSI Electromagnetic Theory Symposium (EMTS'16)* (pp. 751–754). Espoo, Finland.
Muinonen, K., Mishchenko, M. I., Dlugach, J. M., Zubko, E., Penttilä, A., & Videen, G. (2012). Coherent backscattering verified numerically for a finite volume of spherical particles. *The Astrophysical Journal*, *760*(118), 11.
Muinonen, K. O., Sihvola, A. H., Lindell, I. V., & Lumme, K. A. (1991). Scattering by a small object close to an interface. II: Study of backscattering. *Journal of the Optical Society of America A*, *8*, 477–482.
Press, W. H., Teukolsky, S. A., Vetterling, W. T., & Flannery, B. P. (1992). *Numerical recipes in FORTRAN. The art of scientific computing* (2nd ed.). New York: Cambridge University Press.
Shkuratov, Y. G. (1985). *Astronomicheskii Tsircular 1400, 3*. Moscow: Shternberg State Astronomical Institute.
Tsang, L., & Ishimaru, A. (1987). Radiative wave equations for vector electromagnetic propagation in dense nontenuous media. *Journal of Electromagnetic Waves and Applications*, *1*(1), 59–72.
Tsang, L., Kong, J. A., & Shin, R. T. (1985). *Theory of Microwave Remote Sensing*. New York: Wiley.
Videen, G., & Muinonen, K. (2015). Light-scattering evolution from particles to regolith. *Journal of Quantitative Spectroscopy and Radiative Transfer*, *150*, 87–94.
Virkki, A., Markkanen, J., Tyynelä, J., Peltoniemi, J. I., & Muinonen, K. (2015). Polarization by clusters of spherical particles at backscattering. *Optics Letters*, *40*(15), 3663–3666.
Ylä-Oijala, P., Markkanen, J., Järvenpää, S., & Kiminki, S. P. (2014). Surface and volume integral equation methods for time-harmonic solutions of Maxwell's equations. *Progress In Electromagnetics Research*, *149*, 15–44.
Zurk, L. M., Tsang, L., Ding, K. H., & Winebrenner, D. P. (1995). Monte Carlo simulations of the extinction rate of densely packed spheres with clustered and nonclustered geometries. *Journal of the Optical Society of America A*, *12*, 1772–1781.